Nutlin-3a Enhances Natural Killer Cell–Mediated Killing of Neuroblastoma by Restoring p53-Dependent Expression of Ligands for NKG2D and DNAM-1 Receptors

Irene Veneziani[1], Paola Infante[2], Elisa Ferretti[3,4], Ombretta Melaiu[1], Cecilia Battistelli[5,6], Valeria Lucarini[1], Mirco Compagnone[1], Carmine Nicoletti[5,7], Aurora Castellano[1], Stefania Petrini[8], Marzia Ognibene[9], Annalisa Pezzolo[9], Lucia Di Marcotullio[5,6], Roberto Bei[10], Lorenzo Moretta[11], Vito Pistoia[11,†], Doriana Fruci[1], Vincenzo Barnaba[5,12], Franco Locatelli[1,13], and Loredana Cifaldi[1,10,14]

ABSTRACT

In this study, we explored whether Nutlin-3a, a well-known, nontoxic small-molecule compound antagonizing the inhibitory interaction of MDM2 with the tumor suppressor p53, may restore ligands for natural killer (NK) cell–activating receptors (NK-AR) on neuroblastoma cells to enhance the NK cell–mediated killing. Neuroblastoma cell lines were treated with Nutlin-3a, and the expression of ligands for NKG2D and DNAM-1 NK-ARs and the neuroblastoma susceptibility to NK cells were evaluated. Adoptive transfer of human NK cells in a xenograft neuroblastoma-bearing NSG murine model was assessed. Two data sets of neuroblastoma patients were explored to correlate p53 expression with ligand expression. Luciferase assays and chromatin immunoprecipitation analysis of p53 functional binding on *PVR* promoter were performed. Primary neuroblastoma cells were also treated with Nutlin-3a, and neuroblastoma spheroids obtained from one high-risk patient were assayed for NK-cell cytotoxicity. We provide evidence showing that the Nutlin-3a–dependent rescue of p53 function in neuroblastoma cells resulted in (i) increased surface expression of ligands for NK-ARs, thus rendering neuroblastoma cell lines significantly more susceptible to NK cell–mediated killing; (ii) shrinkage of human neuroblastoma tumor masses that correlated with overall survival upon adoptive transfer of NK cells in neuroblastoma-bearing mice; (iii) and increased expression of ligands in primary neuroblastoma cells and boosting of NK cell–mediated disaggregation of neuroblastoma spheroids. We also found that p53 was a direct transcription factor regulating the expression of PVR ligand recognized by DNAM-1. Our findings demonstrated an immunomodulatory role of Nutlin-3a, which might be prospectively used for a novel NK cell–based immunotherapy for neuroblastoma.

Introduction

Neuroblastoma, the most common extracranial tumor of childhood, is still challenging, with the 3-year event-free survival rate lower than 40%, despite intensive multimodal therapies (1). Thus, new treatment strategies are warranted, mainly aimed to restore impaired antitumor immune responses against neuroblastoma (2–4). Indeed, neuroblastoma evades natural killer (NK) cell–mediated innate immunosurveillance through the downregulation of ligands for NK cell–activating receptors (NK-AR; refs. 3, 5, 6). The restoration of the expression of such ligands represents a strategic approach to boost NK cell–mediated antitumor responses against neuroblastoma. Interestingly, whereas ULBP1, ULBP2, and ULBP3 ligands for the NKG2D receptor are known to be regulated by c-MYC and p53 transcription factors (7, 8), no mechanism regulating the expression of ligands for DNAM-1 receptor have been reported so far. Of note, wild-type p53 is found in most neuroblastoma cases, with a rare exception with relapse (9). However, p53 is functionally impaired due to *MYCN* amplification, one of the major neuroblastoma prognostic factors (1), that upregulates not only p53 but also the p53-antagonist MDM2 (10–12). Accordingly, we previously found that the MYCN expression inversely correlated with expression of ligands for both NKG2D and DNAM-1 NK-ARs in neuroblastoma (3). The BET-bromodomain inhibitor JQ1-dependent repression of MYCN leads to downregulation of both c-MYC and p53, resulting in the impaired expression of ligands for both NKG2D and DNAM-1 NK-ARs, thus rendering neuroblastoma cell lines more resistant to NK cell–mediated killing (13).

Nutlins are nontoxic, small-molecule antagonists of p53–MDM2 interactions, known to restore p53-mediated cell-cycle arrest and apoptosis in tumors (14). Among the MDM2-targeting compounds,

[1]Department of Paediatric Haematology/Oncology and of Cell and Gene Therapy, Ospedale Pediatrico Bambino Gesù, IRCCS, Rome, Italy. [2]Center for Life NanoScience@Sapienza, Istituto Italiano di Tecnologia, Rome, Italy. [3]Department of Experimental Medicine, University of Genoa, Genova, Italy. [4]Centre of Excellence for Biomedical Research, University of Genoa, Genova, Italy. [5]Istituto Pasteur-Fondazione Cenci Bolognetti, Rome, Italy. [6]Department of Molecular Medicine, Sapienza University of Rome, Rome, Italy. [7]DAHFMO-Unit of Histology and Medical Embryology, Sapienza University of Rome, Rome, Italy. [8]Confocal Microscopy, Core Facility, Research Laboratories, Ospedale Pediatrico Bambino Gesù, IRCCS, Rome, Italy. [9]Laboratorio Cellule Staminali Post Natali e Terapie Cellulari, IRCCS Giannina Gaslini Institute, Genoa, Italy. [10]Department of Clinical Sciences and Translational Medicine, University of Rome "Tor Vergata," Rome, Italy. [11]Department of Immunology, Bambino Gesù Children's Hospital, IRCCS, Rome, Italy. [12]Cellular and Molecular Immunology Unit, Dipartimento di Scienze Cliniche, Internistiche, Anestesiologiche e Cardiovascolari, Sapienza University of Rome, Rome, Italy. [13]Department of Pediatrics, Sapienza University of Rome, Rome, Italy. [14]Academic Department of Pediatrics (DPUO), Ospedale Pediatrico Bambino Gesù, IRCCS, Rome, Italy.

Note: Supplementary data for this article are available at Cancer Immunology Research Online (http://cancerimmunolres.aacrjournals.org/).

P. Infante and E. Ferretti contributed equally to this article.

†Deceased.

Corresponding Author: Loredana Cifaldi, Department of Clinical Sciences and Translational Medicine, University of Rome "Tor Vergata," Rome, Italy. Phone: 39-06-72596520; E-mail: cifaldi@med.uniroma2.it

Cancer Immunol Res 2021;9:170–83

doi: 10.1158/2326-6066.CIR-20-0313

Nutlin-3a has been mainly explored for its promising therapeutic potential in preclinical studies of leukemia, multiple myeloma, rhabdomyosarcoma (15–22), and neuroblastoma cell lines (21, 23–27). The clinical adoption of several Nutlin-3a analogues is currently under clinical investigation not only in hematologic malignancies, but also in several solid tumors such as sarcoma, glioblastoma, Merkel cell carcinoma, small-cell lung cancer, and breast cancer (https://clinicaltrials.gov/). The molecular characteristics of nontoxicity, cell permeability, and the wide spectrum of antitumor functions render Nutlin-3a, and its analogues, optimal candidates for new therapeutic approaches in neuroblastoma. In light of these pieces of evidence, we investigated whether the rescue of p53 activity by Nutlin-3a could enhance the expression of ligands for NKGD2 and DNAM-1 NK-ARs and, as a consequence, the NK cell–mediated recognition and killing of neuroblastoma.

Materials and Methods

Patient samples

The study was conducted in accordance with the Declaration of Helsinki. Bone marrow (BM) aspirates from 26 neuroblastoma patients diagnosed at onset in our institute and off therapy were used to isolate primary tumor cells for *in vitro* experiments with Nutlin-3a as described below. Tumor samples from 36 neuroblastoma patients diagnosed in our institute were used for NanoString assays. For each patient, written informed parental consent and approval by the Ethical Committee of the Institution were obtained. Demographic, molecular, and histologic features of the cases studied for *in vitro* experiments are detailed in **Table 1**. Staging and histologic classification were performed according to the International Neuroblastoma Staging System (INSS) and the International Neuroblastoma Pathology Classification (INPC; refs. 28, 29), respectively. *MYCN* expression was evaluated following current guidelines (30), and together with *MDM2, TP53, MYC*, and *ALK* gene status was measured by array comparative genomic hybridization (a-CGH) or interphase quantitative fluorescence *in situ* hybridization (IQ-FISH) assays (as described in **Table 1** and below). Neuroblastoma samples were stored in the BIT-neuroblastoma Biobank of IRCCS and obtained before treatment at the time of diagnosis. Tumor content was confirmed by local pathologists' reviews of hematoxylin and eosin–stained tumor sections. Tumor DNA was extracted from fresh neuroblastoma tissue using the MasterPure DNA Purification Kit (Epicentre-Illumina), according to the manufacturer's instructions.

The correlation analysis between p53 and ligands for NK-ARs was evaluated in a cohort of 143 neuroblastoma patients (Target 2018) available at cBioportal.org (www.bioportal.org). Bioinformatic analysis was performed by the Transcription Factor Affinity Prediction (TRAP) website (http://trap.molgen.mpg.de/cgi-bin/home.cgi).

Neuroblastoma cell lines, primary neuroblastoma cells, NK cells, and reagents

Human neuroblastoma cell lines were obtained as follows: SK-N-AS, SH-SY5Y, and SK-N-BE(2)c from the ATCC; LA-N-5 from the Leibniz-Institut DMSZ; SMS-KCNR from Children's Oncology Group Cell Culture. All neuroblastoma cell lines were characterized by (i) HLA class I typing by PCR-SSP sets (Genovision) according to the instructions of the manufacturer, and (ii) array CGH (see below). The human erythro-leukemia cell line K562 was purchased from ATCC and used as a control target for NK cell functional assays. Cells were grown in RPMI-1640 medium supplemented with 10% FBS (Thermo Fisher Scientific), 2 mmol/L glutamine, penicillin (100 mg/mL), and streptomycin (50 mg/mL; Euro Clone S.p.a.). Neuroblastoma cell lines have been reauthenticated by BMR Genomics through PowerPlex Fusion System kit (Promega) and Applied Biosystem 3130XL (Life Technologies). Cell lines were kept frozen in liquid nitrogen, and after thawing, they were cultured for 2 to 3 weeks and passed 4 to 6 times before experimental use. All cell lines were routinely checked for the *Mycoplasma* contamination prior to the use.

Nutlin-3a (Cayman Chemical) was dissolved in DMSO (10 mmol/L) and diluted in medium at the indicated doses for the *in vitro* experiments, or dissolved in ethanol (25 mg/mL) and diluted for the indicated concentration in 2-hydroxypropyl-β-cyclodextrin [HPβCD (SIGMA), 1 g/10 mL H_2O + 1% DMSO], which was also used alone as a vehicle control for *in vivo* experiments.

Primary neuroblastoma cells were isolated from BM aspirates of neuroblastoma patients by depleting $CD45^+$ cells with RosetteSep human CD45 depletion cocktail (cat. #15162; STEMCELL Technologies), followed by Ficoll-Paque Plus (Lympholyte Cedarlane) centrifugation, which allowed to negatively select primary neuroblastoma cells with a purity of about 90% ($GD2^+$) as evaluated by flow cytometry. Primary neuroblastoma cells were resuspended at 2×10^6 cells/mL in RPMI (supplemented as above) with 20% FBS and cultured at 200 μL/well in 96-well flat-button plates. All primary neuroblastoma cells grew in adherence with monolayer distribution, with the exception of those isolated from patient 1 (p1) which formed spheroids. After 5 days, the medium was refreshed, and at 10 to 12 days, cells were treated with 2 μmol/L of Nutlin-3a for 48 hours for *in vitro* experiments. The spheroids of p1 were split twice after 12 days of culture in 96-well flat-button plates, treated with 2 μmol/L of Nutlin-3a for 48 hours or DMSO as control (four wells per condition), and evaluated using an optical microscope (Leica) before and after coculture with 200×10^3 human NK cells/well (see below).

Human NK cells were isolated from peripheral blood mononuclear cells (PBMC) of healthy volunteers with the RosetteSep NK-cell enrichment cocktail (cat. # 15065, STEMCELL Technologies), followed by Ficoll-Paque Plus centrifugation, which allowed to negatively select NK cells with a purity of about 98% ($CD3^-CD56^+$) as evaluated by flow cytometry. NK cells were routinely checked, for the expression of NKG2D and DNAM-1–activating receptors, and NKG2A, KIR2DL1, KIR2DL3, and KIR3DL1 inhibitory receptors by flow cytometry. NK cells with purity greater than 90% and positive for all four inhibitory receptors were resuspended in NK MACS medium (Miltenyi Biotec) supplemented with NK MACS Supplement, human AB serum, and recombinant human IL2 (500 IU/mL; PeproTech). NK cells were cultured at 37°C, split every 3 days, and used up to 20 days after isolation for both *in vitro* and *in vivo* experiments. All NK-cell function assays were performed in an alloreactivity setting (31, 32).

Plasmid construction, transfection, and luciferase reporter assay

The *PVR*-promoter regions spanning from nucleotide (nt) 879 upstream of the transcriptional start site (TSS; corresponding to nt 622–1501 of the *PVR*-promoter sequence) or nt 437 upstream of the TSS (corresponding to nt 1064–1501 of the *PVR* promoter, deleted for the predicted p53 binding sites, spanning from 879 to 437 upstream the TSS) were cloned into the pGL3-basic vector (Promega) by adding BglII and HindIII restriction sites upstream and downstream of the sequences, respectively (sequences and schemes of cloned *PVR*-promoter regions in Supplementary Table S1). The plasmids were named as pGL3-*PVR* promoter (*PVR* promoter) and pGL3-*PVR* promoter p53-deleted (*PVR* promoter p53-deleted), respectively. The pRL-TK vector (Promega) was used as an internal reference in the luciferase reporter system. An empty pGL3 (basic) was used as a negative control. Plasmids were transfected into LA-N-5 cells using Lipofectamine 2000 (Invitrogen). The day before

Table 1. Diagnostic characteristics and status of *MYCN, MDM2, TP53, MYC*, and *ALK* in NB patients.

Patient number	Age	INSS stage	INRG stage	Subtype	Differentiation grade	Tumor site	*MYCN*	*MDM2*	*TP53*	*MYC*	*ALK*	Tumor cell number/mL of BM	Primary tumor cell growth	Follow-up	Disease state
p1	2y 5m	4	M	NB	SD	Retroperitoneum	amp	sc	gain	sc	amp	3.5×10^6	Yes	Dead	—
p2	3y	4	M	NB	SD	Adrenal gland	amp	sc	sc	sc	sc	2.1×10^6	Yes	Dead	—
p3	3y	4	M	NB	SD	Adrenal gland	amp	sc	sc	sc	sc	1.7×10^6	Yes	Alive	CR
p4	3y 9m	4	M	NB	SD	Adrenal gland	gain	sc	sc	sc	gain	1.8×10^6	Yes	Alive	SRD
p5	2y 8m	4	M	NB	SD	Retroperitoneum	gain[a]	nd	nd	nd	nd	2.0×10^6	Yes	Dead	—
p6	4y 2m	4	M	NB	SD	Adrenal gland	gain[a]	nd	nd	nd	nd	1.4×10^6	No	Alive	CR
p7	2m	4	M	NB	SD	Thoracic cavity	sc	sc	gain	delete	sc	1.7×10^6	No	Alive	CR
p8	3y 7m	4	M	NB	SD	Thoracic cavity	sc[a]	nd	nd	nd	nd	3.0×10^6	Yes	Alive	SRD
p9	8y	4	M	NB	SD	Adrenal gland	sc[a]	nd	nd	nd	nd	$0,7 \times 10^6$	No	Dead	—
p10	2y 9m	4	M	NB	SD	Adrenal gland	sc[a]	nd	nd	nd	nd	1.5×10^6	No	Alive	CR
p11	15y	4	M	NB	SD	Retroperitoneum	nd	nd	nd	nd	nd	0.6×10^6	No	Alive	SRD
p12	5y 1m	4	M	NB	SD	Adrenal gland	nd	nd	nd	nd	nd	0.6×10^6	No	Alive	SRD
p13	5y 6m	4s	Ms	GNBL	Nodular	Retroperitoneum	sc	gain	sc	sc	sc	1.0×10^6	No	Alive	AD
p14	3m	4s	Ms	NB	SD	Adrenal gland	gain	gain	gain	gain	gain	1.7×10^6	Yes	Alive	SRD
p15	7m	3	L2	NB	SD	Adrenal gland	gain[a]	nd	nd	nd	nd	1.5×10^6	No	Alive	CR
p16	1y 4m	3	L2	NB	SD	Retroperitoneum	gain	sc	gain	sc	gain	1.2×10^6	No	Alive	SRD
p17	1y 9m	3	L2	NB	SD	Retroperitoneum	sc	sc	sc	sc	sc	2.0×10^6	No	Alive	CR
p18	5y 5m	2A	L2	NB	SD	Thoracic cavity	sc[a]	nd	nd	nd	nd	0.3×10^6	No	Alive	AD
p19	9m	2B	L2	NB	SD	Adrenal gland	sc	sc	sc	gain	sc	$0,7 \times 10^6$	No	Alive	SRD
p20	2y 10m	1	L1	GNBL	Nodular	Neck	amp[a]	nd	nd	nd	nd	2.2×10^6	Yes	Alive	CR
p21	4y	1	L1	NB	SD	Thoracic cavity	sc	gain	sc	sc	sc	1.4×10^6	No	Alive	CR
p22	9m	1	L1	NB	SD	Sacrococcygeal region	sc[a]	nd	nd	nd	nd	0.8×10^6	No	Alive	CR
p23	2y 1m	1	L1	NB	SD	nd	nd	nd	nd	nd	nd	1.1×10^6	No	Alive	CR
p24	7m	1	L1	NB	SD	Adrenal gland	sc	sc	sc	sc	sc	0.6×10^6	No	Alive	CR
p25	4y 1m	1	L1	GNBL	Nodular	Retroperitoneum	nd	nd	nd	nd	nd	1.6×10^6	Yes	Alive	CR
p26	3y 7m	1	L1	Not classified	Not classified	Thoracic cavity	nd	nd	nd	nd	nd	0.5×10	No	Alive	CR

Abbreviations: AD, active disease; amp, amplified; CR, complete remission; GNBL, ganglioneuroblastoma; INRG, International Neuroblastoma Risk Group; INSS, International Neuroblastoma Staging System; NB, neuroblastoma; nd, not determined; sc, single copy; SD, scarcely differentiated; SRD, stable residual disease.
[a]Evaluated by FISH array.

transfection, cells were seeded in 12-well plates. At 80% confluency, the plasmids were transiently transfected according to the manufacturer's protocol. For each well, 1 μg of the luciferase-containing plasmid [pGL3-*PVR* promoter (*PVR* promoter) and pGL3-*PVR* promoter p53-deleted (*PVR* promoter p53-deleted)] and 0.07 μg of the renilla-containing plasmid pRL-TK vector (Promega) were used. All transfections were carried out in quadruplicate. After 24 hours, cells were lysed with passive lysis buffer (Promega), and both renilla and firefly luciferase activities were measured by using a Triathler Multilabel Tester (Hidex), after incubation with the relative Dual Luciferase Reporter Assay System reagents (Promega) according to the manufacturer's protocol. The luciferase activity relative to renilla was represented as mean ± standard error of mean (SEM).

Xenograft neuroblastoma model and treatment of neuroblastoma-bearing NSG mice

All animal experiments were performed in accordance with a protocol approved by the Italian Ministry of Health and our institutional animal care. All *in vivo* experiments utilized 4- to 6-week-old female NSG (NOD. Cg-Prkdcscid IL2rgtm1Wjl/SzJ) mice (Charles River Laboratories Italia srl). Briefly, 5×10^6 cells LA-N-5 neuroblastoma cells resuspended in 100 mL PBS were injected subcutaneously into flank of mice (33). Neuroblastoma-bearing NSG mice were used for both the *in vivo* experiments to evaluate the effectiveness of Nutlin-3a in inducing both ligand expression and NK cell–mediated antitumor activity. In the first experiment, 20 to 25 days after the injection of LA-N-5, when tumor masses reached about 50 mm^3, LA-N-5–bearing NSG mice were randomly divided in three groups (six mice for each group): control group mice were injected intraperitoneally (i.p.) with vehicle for Nutlin-3a or HPβCD; experimental group mice were injected with 20 mg/kg (mg of Nutlin-3a/mouse body weight) and 40 mg/kg Nutlin-3a, every 2 days for 12 days. At the end of the treatment, about 35 days after the LA-N-5 injection, tumor masses were harvested and used for photo acquisition and IHC analysis as described below. In another set of experiments, LA-N-5–bearing NSG mice were randomly divided into groups of six mice. For controls, mice were injected with HPβCD (i.p. as vehicle in place of Nutlin-3a) and with PBS (peritumoral as vehicle in place of NK cells; i.p. as vehicle in the place of IL2). For treatments, LA-N-5–bearing NSG mice were divided into five groups (g): vehicles only (i.p. HPβCD and both i.p. and peritumoral PBS, g1); i.p. IL2 and vehicles (i.p. HPβCD and peritumoral PBS, g2); i.p. Nutlin-3a and vehicles (both peritumoral and i.p. PBS, g3); peritumoral human NK cells, i.p. IL2, and vehicle (i.p. HPβCD, g4); i.p. Nutlin-3a, peritumoral NK cells, and i.p. IL2 (g5). In the experimental groups g3 and g5, 20 to 25 days after the injection of LA-N-5, when tumor masses reached about 50 mm^3, mice were injected i.p. with Nutlin-3a (40 mg/kg) every 2 days for 2 weeks. In the experimental groups g4 and g5, 5×10^6 of NK cells were peritumorally injected after 48 hours of the first Nutlin-3a treatment and every 5 days for 2 weeks. In the experimental groups g2 and g5, IL2 (10×10^3 U/mouse) was injected i.p. the same day of NK-cell injection and for another consecutive 3 days. Three treatment cycles were performed for each experiment. Tumor size was assessed every 2 days by caliper measurement. At the end of treatment, 55 to 60 days after LA-N-5 injection or 35 days after the start of treatment, tumor masses from g1, g2, g3, g4, and g5 mice were harvested and used for photo acquisition and IHC analysis as described below. For overall survival experiments, mice were kept alive for up to nearly 50 days or sacrificed when tumor masses reached almost 2 cm^3.

Antibodies, flow cytometry, apoptosis, and Western blotting

The following antibodies for flow cytometry, with clones indicated in parentheses, were used: anti–GD2-Alexa Fluor-647 (14.G2a), anti–CD107a-FITC (H4A3), anti–CD3-Alexa Fluor-700 (UCHT1), anti–CD56-PE-Cy7 (B159), anti-CD45 (HI30), anti–NKG2D-BV605 (1D11) purchased from BD Biosciences; anti–DNAM-1-APC (11A8) purchased from BioLegend; anti-TIGIT (MBSA43) purchased from eBioscience; anti–KIR2DL1/2DS1-PC5.5 (EB6B), anti–KIR2DL2/L3/S2-PE (GL-183) purchased from Beckman Coulter; anti–NKG2A-Alexa Fluor-700 (131411), anti–KIR3DL1-APC (DX9), anti–ULBP1-PE (170818), anti–ULBP2/5/6-PE (165903), anti–ULBP3-PE (166510), anti-MICA (159227), anti-MICB (236511), anti–TRAIL/R2-APC (17908), anti–CD155/PVR-PE (300907), anti–Nectin-2/CD112-APC (610603) purchased from R&D Systems; and goat F(ab')2 Fragment anti-mouse IgG FITC (IM1619) purchased from Dako. All these antibodies were used at the concentrations according to the manufacturers' protocol. Apoptosis of tumor cells was evaluated with APC-conjugated Annexin V (BD-Pharmingen) and propidium iodide (PI; Sigma-Aldrich), used at the concentration according to the manufacturer's protocol and analyzed by flow cytometry. Flow cytometry was performed on FACSCantoII and LSRFortessa (BD Biosciences) and analyzed by FlowJo Software.

The following antibodies for IHC, with clones indicated in parentheses, were used: anti-PVR (NBP1-88131) purchased from Space, anti–Nectin-2 (62540) purchased from Abcam, and anti-NKp46/NCR1 (195314) purchased from R&D Systems. All these antibodies were used at the concentration according to the manufacturer's protocol.

Human whole-cell extracts were quantified by a bicinchoninic acid assay (Thermo Fisher Scientific), resolved on 8% to 10% SDS-PAGE, and electroblotted. Filters were probed with primary antibodies for 3 hours at room temperature or overnight at 4°C, followed by goat anti-mouse HRP-conjugated IgG (code 115-035-003, Jackson ImmunoResearch) at a 1:10,000 milk dilution (34). The following antibodies for Western blotting, with clones and milk dilution, respectively, indicated in parentheses, were used: anti-MYCN (B8.4.B, 1:200), anti-p53 (FL-393, 1:200), anti-p21 (C-19, 1:200), anti-Actin (I-19, 1:1,000), all from Santa Cruz Biotechnology; anti-MDM2 (2A10, 1:1,000) was from Calbiochem-Millipore.

A-CGH and IQ-FISH

DNA from human neuroblastoma primary tumors was tested by high-resolution a-CGH. The tests involved the use of a 4 × 180K platform (Agilent Technologies) with a mean resolution of approximately 25 kb. A copy-number variant was defined as a displacement of the normal value of at least eight consecutive probes and the mapping positions refer to the Genome Assembly GRCh38/hg19 (UCSC Genome Browser, http://genome.ucsc.edu, February 2009 release). The data were analyzed using the Genomic Workbench 7.0.40 software (Agilent), the altered chromosomal regions and breakpoints events were detected using ADM-1 mathematical algorithm (threshold 10), with a 0.5-Mb window size to reduce false positives. The quality of the test was assessed on the strength of the QCmetrics values. Polymorphisms (http://dgv.tcag.ca/dgv/app/home) were not included because they were considered normal variants. The data generated in this study have been deposited in the Gene Expression Omnibus (GEO) database under the accession number GSE145341.

IQ-FISH (35–37) was performed on 4-μm-thick paraffin-embedded neuroblastoma tissue sections from patients 5, 6, 8, 9, 10, 15, 18, 20, and 22. Dual-color FISH probes containing *MYCN* (2p24) and *LAF* (2q11) control probes (labeled green; Kreatech Biotechnology) were used to assess *MYCN* gene status (amplified, not amplified) as recommended by the International Neuroblastoma Risk Group Biology Committee. The samples were imaged using the

fluorescence microscope Axio Imager M2 equipped with ApoTome System (Carl Zeiss).

Quantitative mRNA expression

Total human RNA was extracted using TRIzol Reagent (Thermo Fisher Scientific), and 1 μg was used to synthesize first-strand cDNA using the SuperScript II First-Strand cDNA synthesis kit (Thermo Fisher Scientific). Quantitative real-time PCR (qPCR) reactions were performed using prevalidated TaqMan gene-expression assays (Hs00197846_m1 for *PVR*), and QuantStudio 6 Flex Real-time PCR System machine from Applied Biosystems, Thermo Fisher Scientific. Relative gene expression was determined using the $2^{-\Delta\Delta Ct}$ method, and $2^{-\Delta Ct}$ considered as expression, with *GAPDH* (Hs02758991_g1) as the endogenous control.

Chromatin immunoprecipitation analysis

LA-N-5 cells were cultured in cell culture dishes and at 80% confluency, were treated with DMSO as control or with Nutlin-3a (2 μmol/L) for 16 hours. The cells were then treated with formaldehyde (1% final concentration) for 10 minutes at room temperature, by adding it directly to the culture dishes, to cross-link protein complexes to the DNA. The reaction was stopped by adding glycine to a final concentration of 0.125 mol/L for 5 minutes at 4°C. Cells were washed with cold PBS, scraped, and lysed in L1 buffer [2 mmol/L EDTA, 50 mmol/L Tris-HCl (pH 8.1), 0.1% NP40, 10% glycerol, and cOmplete, EDTA-free Protease Inhibitor Cocktail according to the manufacturer's instructions] for 20 minutes at 4°C in rotation. The lysates were homogenized using 15 dounce-homogenizer strokes and then centrifuged at 5,000 rpm for 5 minutes at 4°C. Nuclear pellets were resuspended in L2 buffer (5 mmol/L EDTA, 50 mmol/L Tris-HCl (pH 8.0), 1% SDS, and cOmplete, EDTA-free Protease Inhibitor Cocktail according to the manufacturer's instructions) and kept for 20 minutes at 4°C in rotation. Nuclear lysates were sonicated with a Vibra-Cell Ultrasonic Liquid Processor to obtain chromatin fragments of an average length of 200 to 500 bp and centrifuged at 10,000 rpm for 10 minutes at 4°C. After determining DNA concentrations, each chromatin sample was divided into aliquots of 150 μg. The sonicated supernatant fractions were diluted 10-fold with dilution buffer [5 mmol/L EDTA, 50 mmol/L Tris-HCl (pH8.0), 0.5% NP40, 200 mmol/L NaCl, and cOmplete EDTA-free Protease Inhibitor Cocktail according to the manufacturer's instructions]. For each condition, one aliquot for the specific antibody (anti-p53, BK9282S CST, EuroClone) and one aliquot for the IgG control (BK2729S CST, EuroClone) were incubated with 40 μL Protein A Sepharose (GE Healthcare), saturated with 3% BSA and 200 μg/mL salmon sperm, for 3 hours at 4°C on a rotating platform. The precleared chromatin samples were centrifuged at 13,000 rpm for 30 seconds and incubated with 5 μg of the respective antibody or IgG overnight with gentle rotation at 4°C. Immunoprecipitated samples were recovered by incubation with 50 μL saturated Protein A Sepharose (GE Healthcare) on a rotating platform for 3 hours at 4°C. Before washing, the supernatant of the IgG control was taken as an input sample. After extensive washing (5 minutes at 4°C in rotation and subsequent centrifugation at 3,000 rpm for 2 minutes) with wash buffers [2 washes with 0.1% SDS, 1% Triton X-100, 2 mmol/L EDTA, 20 mmol/L Tris-HCl (pH 8.1), 150 mmol/L NaCl; 2 washes with 0.1% SDS, 1% triton X-100, 2 mmol/L EDTA, 20 mmol/L Tris-HCl (pH 8.1), 500 mmol/L NaCl; 1 wash with 0.25 ml/L LiCl, 1% NP40, 1% deoxycholate, 1 mmol/L EDTA, 10 mmol/L Tris-HCl (pH 8.1); 1 wash with 10 mmol/L Tris-HCl, 1 mmol/L EDTA (pH 8.0)], samples were eluted in elution buffer (100 mmol/L NaHCO3, 1% SDS) at room temperature twice while vortexing for 15 minutes. After each elution, samples were centrifuged at 13,000 RPM for 5 minutes, and the eluate was collected. The samples were treated with 10 μg RNAse A (Sigma-Aldrich) for 10 minutes at room temperature and incubated at 67°C overnight to reverse the protein–DNA cross-linking. In each sample, $NaHCO_3$ was neutralized with 6 μL Tris-HCl 1 mol/L (pH 6–7.5). After treatment with proteinase K (Sigma-Aldrich) for 2 hours at 56°C, DNA was extracted with phenol-chloroform (Invitrogen), precipitated with 100% ethanol, and resuspended in 50 μL of distilled water. Five nanograms of the immunoprecipitated, IgG, and input samples was used for PCR with specific oligonucleotides spanning the *PVR* promoter: PVR P 53BS 3F AGGCTGGTCTTGAACTCCTG and PVR P 53BS 3R CCATTGCGCCACTACACTAC. The reaction was performed in triplicate using 5 ng of DNA, GoTaq qPCR Master Mix (Promega), and the relative qPCR primer pair in the thermocycler, CFX Connect Real-time PCR detection system (Bio-Rad). The primer pair efficiency, the relative quantity of each immunoprecipitated and IgG (ΔC(t)) with respect to the input sample, and the SEM of the relative quantity were determined with CFX ManagerTM software (Bio-Rad). The percentage of the relative quantity of each immunoprecipitated sample was normalized with respect to IgG and expressed as a percentage of input chromatin (% input).

NanoString assay

Total RNA was extracted from 36 fresh frozen neuroblastoma samples using the Total RNA Purification Plus Kit (Norgen, Biotek Corp. Thorold) and purified with the RNA Cleanup and Concentration kit (Norgen, Biotek Corp. Thorold). RNA concentration was measured with Nanodrop 2000 (Thermo Scientific), whereas RNA integrity and purity was evaluated with the RNA Bioanalyzer kit (Agilent Technologies). Differential expression of immune-related gene transcripts was determined using The human NanoString PanCancer Immune Profiling assay (https://www.nanostring.com/resources/gene-expression-panels-flyer/) was used to evaluate the expression of 730 immune-related genes and 40 housekeeping genes according to the manufacturer's protocol (NanoString Technologies, Inc.). Briefly, 8 μL of the NanoString detection probe containing mastermix was incubated overnight with 100 ng of total RNA for each neuroblastoma sample. After hybridization, the samples were loaded into 12-stripe NanoString tubes and placed in the nCounter Prep-station (NanoString) for purification. Gene expression was measured on the NanoString nCounter Analysis System (NanoString Technologies). The raw NanoString RCC files were preprocessed by R/Bioconductor library NanoStringNorm as previously described (38). The data were normalized for (i) the variation of the technical assay with the geometric mean of internal positive controls, (ii) the background count with the mean plus two standard deviations, and (iii) the RNA content with the geometric mean of housekeeping genes, following the manufacturer's recommendations (39). The normalized expression values were transformed into $\log_2$ and used for statistical analysis as described (40).

Cytotoxicity and degranulation assay

NK-cell cytotoxic activity was tested by a standard 4-hour ^{51}Cr-release assay. Briefly, ^{51}Cr [Amersham International; 100 μCi (3.7 MBq)/1 × 10^6 cells]-labeled K562 or neuroblastoma target cells (5 × 10^3) were mixed with human NK cells from healthy donors at different effector–target (E:T) cell ratios and incubated at 37°C. After 4 hours of incubation, 25 μL supernatant were removed, and the ^{51}Cr release was measured with a TopCount NXT beta detector (PerkinElmer

Life Sciences). All experimental groups were analyzed in triplicate, and the percentage of specific lysis by counts per minute (cmp) was determined as follows: 100× (mean cpm experimental release − mean cpm spontaneous release)/(mean cpm total release − mean cpm spontaneous release). Specific lysis was converted to lytic units (L.U.) calculated from the curve of the percentage lysis. One lytic unit was defined as the number of NK cells required to produce 20% lysis of 10^6 target cells during the 4-hour incubation.

Degranulation assays were performed by coculturing human NK cells from healthy donors with K562 or neuroblastoma target cells at 1:1 ratio for 3 hours in complete medium in the presence of anti-CD107a (diluted 1:100). In the last 2 hours, GolgiStop (BD Bioscience) at a 1:500 dilution was added. Cells were then stained with anti-CD56 and anti-CD45 (both diluted 1:50), and the expression of CD107a was evaluated by flow cytometry in the $CD56^+CD45^+$ subset. In the blocking experiments, NK cells were pretreated for 20 minutes with 25 μg/mL of neutralizing anti-NKG2D (149810, R&D Systems) and anti–DNAM-1 (DX11, BD-Pharmingen), at room temperature before coculture with target cells.

IHC and live-cell imaging

Tumor masses from LA-N-5–bearing NSG mice were formaldehyde fixed, paraffin embedded, cut into 3-μm sections, and baked for 60 minutes at 56°C in a dehydration oven. Antigen retrieval and deparaffinization were carried out on a PT-Link (Agilent Technologies) using the EnVision FLEX Target Retrieval Solution kits at high pH (Agilent Technologies) for both PVR and Nectin-2, as per the manufacturer's instruction. Slides were then blocked for endogenous peroxidase for 10 minutes with a peroxidase-blocking solution (Agilent Technologies) or the avidin/biotin blocking system (Thermo Fisher Scientific), according to the manufacturer's instructions and then incubated for 30 minutes with 5% PBS/BSA. Slides were subsequently incubated overnight at 4°C with primary antibodies against PVR (1:200), Nectin-2 (1:300), and NKp46 (1:100) and subsequently with secondary antibody coupled to peroxidase (Dako, ready to use) or streptavidin alkaline phosphatase (Dako, ready to use). Bound peroxidase or streptavidin were detected with diaminobenzidine (DAB) and EnVision FLEX substrate buffer containing peroxide (Dako) or with Fast Red chromogen substrate (Dako) solution, respectively. Tissue sections were counterstained with EnVision FLEX hematoxylin (Agilent Technologies), and immunostained slides were acquired using a Nikon microscope [eclipse E600=upright microscope and NanoZoomer S60 digital slide scanner (Hamamatsu)]. IHC density was obtained by evaluating integrated optical density by Color Deconvolution plugin through ImageJ, measured in independent slide images acquired with the same optical microscopic parameters such as magnification, light exposure, and acquisition time. Sections of normal human intestinal mucosa and human colon carcinoma were used as positive controls for PVR and Nectin-2, respectively. As negative controls, slides were processed with the same procedure described above with the exclusion of the primary Ab incubation, before being acquired.

For time-lapse experiments, 5×10^5 of LA-N-5 or SMS-KCNR neuroblastoma cell lines were marked with 1 μmol/L of CellTracker Deep Red (Thermo Fisher Scientific), cultured in cell dishes (Ibidi) ideal for live-cell imaging and high-resolution microscopy, and treated with 2 μmol/L of Nutlin-3a for 48 hours. Then cancer cells were incubated for 15 minutes with 1 μmol/L of CellTracker Deep Red (Thermo Fisher Scientific), a fluorescent dye well suited for tracking of cellular movements, that is retained inside cells through several generations. After removing the CellTracker, human NK cells (2×10^6 cells/mL) from healthy donors as described above were added to cultured cells, and dishes were immediately imaged. Time-lapse acquisitions were performed by a Leica TCS-SP8X laser-scanning confocal microscope (Leica Microsystems) using the 633-nm laser line of a tunable white light laser source for CellTracker Deep Red excitation for cancer cell imaging, and the phase contrast to visualize both tumor and NK cells. Confocal images were acquired with an HC PLAPO CS2 20× objective (0.75 numerical aperture, Leica Microsystems). Z-reconstructions of serial single optical sections were obtained every 30 seconds and carried out with a 512 × 512 format, scan speed of 700 Hz, a zoom magnification up to 1.3, and z-step size of 1 μmol/L. Regions of interest were manually created surrounding each group of fluorescent cancer cells in the maximum intensity projection containing 12 distinct z planes of confocal images using the LAS X (Leica Microsystems) software. The area size variations (expressed in % values) of each cell group, measured before and after NK-cell addition, were compared with area values of cells pretreated with DMSO as control. Acquisition settings (lasers' power, beam splitters, filter settings, pinhole diameters, and scan mode) were the same for all examined samples of each staining. Time-lapse microscopy was performed with a stage incubator (OkoLab, Naples, Italy) to maintain stable conditions of temperature, CO_2, and humidity during live-cell imaging.

Statistical analysis

Digital images of Western blots and IHC were analyzed by ImageJ (http://rsbweb.nih.gov/ij/index.html). Survival data are presented as Kaplan–Meier plots and were analyzed using a log-rank (Mantel–Haenszel) method. For all data, statistical significance was evaluated by the two-tailed unpaired Student t test. Normalized values were analyzed for correlation by the regression analysis using GraphPad software. *P* values not exceeding 0.05 were considered to be statistically significant.

Results

Nutlin-3a effects on ligands for NK-ARs and neuroblastoma cell line susceptibility to NK cells

The treatment of p53-wild-type or p53-mutant neuroblastoma cell lines, including both *MYCN*-amplified and *MYCN* nonamplified neuroblastoma cell lines, with different Nutlin-3a concentrations for 48 hours induced a progressive upmodulation of p53, MDM2, and p21 only in p53-wild-type neuroblastoma cell lines without affecting the MYCN expression (except in LA-N-5 cells at higher doses; Supplementary Fig. S1A and S1B). As expected, highest doses of Nutlin-3a induced apoptosis, particularly in p53-wild-type neuroblastoma cell lines (ref. 41; Supplementary Fig. S2A). The rescue of p53 function by preapoptotic Nutlin-3a concentration induced a significant upregulation of NKG2D receptor ligands ULBP1 and ULBP3 in *MYCN* nonamplified SH-SY5Y cells (Supplementary Fig. S2B), as well as NKG2D receptor ligands ULBP1, ULBP2/5/6, and ULBP3 and DNAM-1 receptor ligands PVR and Nectin-2 in both *MYCN*-amplified LA-N-5 and SMS-KCNR cells (**Fig. 1A**; Supplementary Fig. S2C), without affecting the expression of MICA and MICB in any neuroblastoma cell line analyzed (Supplementary Fig. S2D). Conversely, the expression of ligands for NK-ARs did not change in the p53-mutant neuroblastoma cell lines (Supplementary Fig. S2B).

Experiments were specifically designed to evaluate if the Nutlin-3a–dependent upregulation of ligands for NK-ARs on *MYCN*-amplified neuroblastoma cells could improve NK cell–mediated recognition and killing. Results demonstrated that both LA-N-5 and SMS-KCNR

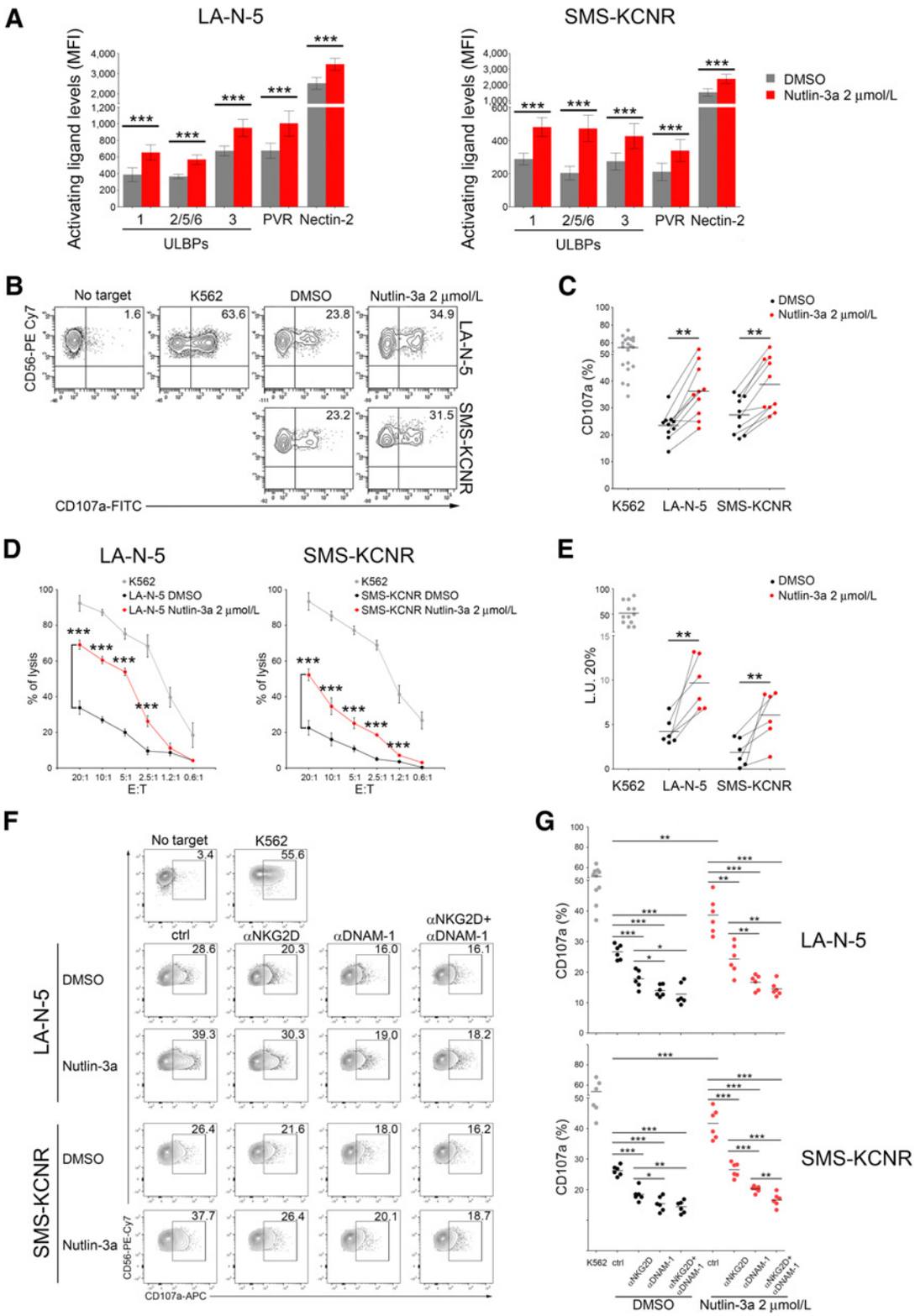

neuroblastoma cells became significantly more susceptible to NK cell–mediated recognition (**Fig. 1B** and **C**) and lysis (**Fig. 1D** and **E**) upon treatment with Nutlin-3a. Blocking experiments demonstrated that DNAM-1, more than NKG2D, was involved in the NK cell–mediated recognition of Nutlin-3a–treated neuroblastoma cells (**Fig. 1F** and **G**). Time-lapse analysis of NK cell–mediated killing of both target cell lines showed that the tumor area of Nutlin-3a–treated neuroblastoma cells underwent a significant gradual contraction, compared with the tumor area of DMSO-treated control cells, after 3 hours of coculture (Supplementary Fig. S3A and S3B; Supplementary Video S1). Nutlin-3a treatment of NK cells did not affect the expression of either NK-ARs or the TIGIT inhibitory receptor, known to compete with DNAM-1 in the binding of the PVR ligand (ref. 42; Supplementary Fig. S4A and S4B), nor did it affect NK-cell degranulation in response to neuroblastoma target cells (Supplementary Fig. S4C). Collectively, these data indicated that Nutlin-3a–mediated p53 rescue increased the susceptibility of neuroblastoma cells to NK cell–mediated killing by inducing the expression of ligands for both NKG2D and DNAM-1 receptors on p53-wild-type neuroblastoma cells.

P53 is a direct transcription factor for PVR-activating ligand

Whereas p53 is known to be a transcription factor for *ULBP1* and *ULBP2* by specifically linking p53-responsive elements to related gene introns (8), whether p53 could act as a transcription factor directly binding the gene promoters of ligands for NK-ARs has not yet been reported. First, we analyzed the possible correlation between p53 and ligands for NKG2D (MICB, ULBP1, ULBP2, and ULBP3) or DNAM-1 (PVR and Nectin-2) in 143 neuroblastoma patients (Target 2018, www.bioportal.org). *TP53* expression significantly correlated with *PVR* expression, but not with the other ligands analyzed (Supplementary Fig. S5A). Bioinformatic analysis by the TRAP website revealed six putative p53 binding sites on the *PVR* promoter, but only one on the *ULBP3* promoter and none on the other ligand promoter tested (Supplementary Fig. S5B and S5C). These data suggest that the p53-mediated induction of the other ligands was independent of the direct p53 binding to the related promoters and requires further studies. The significant correlation between *TP53* and *PVR* expression was confirmed in 36 neuroblastoma patients by NanoString gene analysis (**Fig 2A**). Nutlin-3a significantly induced time-dependent *PVR* mRNA expression in p53-wild-type neuroblastoma cell lines compared with DMSO-treated control cells (**Fig. 2B**). To validate the potential functional binding of p53 to the *PVR* promoter, we performed a dual luciferase reporter assay using two constructs, one containing a *PVR*-promoter region including six putative p53-binding sites and the other deleted of the four putative p53-binding sites furthest away from the TSS, as predicted by bioinformatics analysis (Supplementary Fig. S5C). The deletion of the putative p53-binding sites resulted in significantly reduced luciferase activity, suggesting that p53 might bind to chromatin on the *PVR* promoter, contributing to *PVR* expression (**Fig. 2C**). Last, chromatin immunoprecipitation (ChIP) assays using primers encompassing the *PVR*-promoter region including the higher affinity p53 putative binding site revealed by TRAP, showed that Nutlin-3a favored p53 binding to the *PVR* promoter (**Fig. 2D**), thus indicating that p53 may function as a direct transcription factor for *PVR*.

Nutlin-3a upregulates the expression of ligands for NK-ARs *in vivo*

In order to evaluate the efficacy of Nutlin-3a *in vivo*, we performed murine xenograft experiments (**Fig. 3A**). IHC analyses in sections of neuroblastoma tissues, isolated from LA-N-5–bearing NSG mice, showed a significant increase of both PVR and Nectin-2 expression in tumor masses from mice that had been treated with preapoptotic doses of Nutlin-3a (24) compared with tumor masses from control mice treated with the Nutlin-3a vehicle HPβCD (**Fig. 3B** and **C**; Supplementary Fig. S6A), without affecting both growth and apoptosis rates (Supplementary Fig. S6B).

Nutlin-3a enhances NK cell–mediated killing of *MYCN*-amplified neuroblastoma in tumor-bearing mice

Next, we asked whether the increased expression of ligands for NK-ARs by Nutlin-3a treatment could be effective in improving NK-cell activity against neuroblastoma in neuroblastoma-bearing NSG mice. The combination of Nutlin-3a treatment, human NK-cell transfer, and IL2 boosting (**Fig. 4A**; ref. 43) induced a significant reduction of the tumor growth compared with the various controls, including treatments with HPβCD or PBS (used as both Nutlin-3a and IL2 or NK-cell vehicles, respectively) with or without IL2 (**Fig. 4B** and **C**; Supplementary Fig. S7) or NK cells and IL2 (**Fig. 4B**, last panel). IHC of neuroblastoma tissues, isolated from the five groups of LA-N-5–bearing NSG mice, showed a significant increase of both PVR and Nectin-2 expression only in mice treated with Nutlin-3a compared with other groups, thus excluding an immunomodulatory effect on ligand expression by IL2 and/or NK cells in combination with vehicles (Supplementary Fig. S8A and S8B). These data suggest that Nutlin-3a was able to boost NK cell–mediated killing of neuroblastoma in an *in vivo* animal model. The combined treatment of Nutlin-3a and NK cells significantly improved mouse overall survival, leading to a 50% survival at 50 days of monitoring (**Fig. 4D**).

Subsequent experiments were performed to assess if the reduced tumor size and improved survival of Nutlin-3a/NK cell–treated neuroblastoma-bearing mice were associated with an increase of tumor-infiltrating NK cells. NK cells, detected by the expression of the NK cell–activating receptor NKp46 by IHC, were predominantly present in both peritumoral and internal zones of tumor masses from neuroblastoma-bearing mice treated with the combination of Nutlin-

Figure 1.

Nutlin-3a renders neuroblastoma cell lines more susceptible to NK cell–mediated killing by upregulating the expression of ligands for NK-ARs. **A,** Summary of five independent flow cytometry analyses of surface expression of the indicated ligands for NK-ARs in neuroblastoma cell lines left untreated (DMSO, gray bar) or treated with Nutlin-3a (red bar) at 2 μmol/L for 48 hours. Mean ± SD; ***, $P < 0.001$. MFI, mean fluorescence intensity. **B,** Degranulation of human $CD45^+CD56^+CD3^-$ NK cells from healthy donors, measured as CD107a cell-surface expression upon stimulation with LA-N-5 or SMS-KCNR left untreated (DMSO) or treated with Nutlin-3a at 2 μmol/L for 48 hours. K562 cells were used as a positive control. The percentage of $CD107a^+$ NK cells is indicated. A representative experiment out of the 10 performed is shown. **C,** Summary of the degranulation of NK cells isolated from 10 healthy donors. Dots, percentage of $CD107a^+$ NK cells; horizontal bars, mean; **, $P < 0.01$. **D,** DMSO and Nutlin-3a–treated LAN-5 and SMS-KCNR cell lines were used as targets for NK cells at the indicated E:T ratios in a standard 4-hour ^{51}Cr-release assay. Mean ± SD; ***, $P < 0.001$. **E,** Summary of cytotoxic assay of NK cells isolated from healthy donors. Specific lysis was converted to L.U. 20%. Dots, L.U. 20% of the E:T unpaired tested; horizontal bars, mean; **, $P < 0.01$. **F,** Anti-NKG2D and anti-DNAM-1 neutralization experiments in a degranulation assay of NK cells preincubated with one or both neutralizing anti-NKG2D and anti–DNAM-1 and stimulated with LA-N-5 or SMS-KCNR left untreated (DMSO) or pretreated with Nutlin-3a at 2 μmol/L for 48 hours. K562 cells were used as a positive control. The percentage of $CD107a^+$ NK cells is indicated in each dot plot. A representative experiment of NK cells isolated from one healthy donor out of six performed is shown. **G,** Summary of the neutralization experiments showing degranulation of NK cells isolated from six healthy donors. Dots, percentage of $CD107a^+$ NK cells; horizontal bars, mean; *, $P < 0.05$; **, $P < 0.01$; ***, $P < 0.001$. *P* value (two-tailed unpaired Student *t* test).

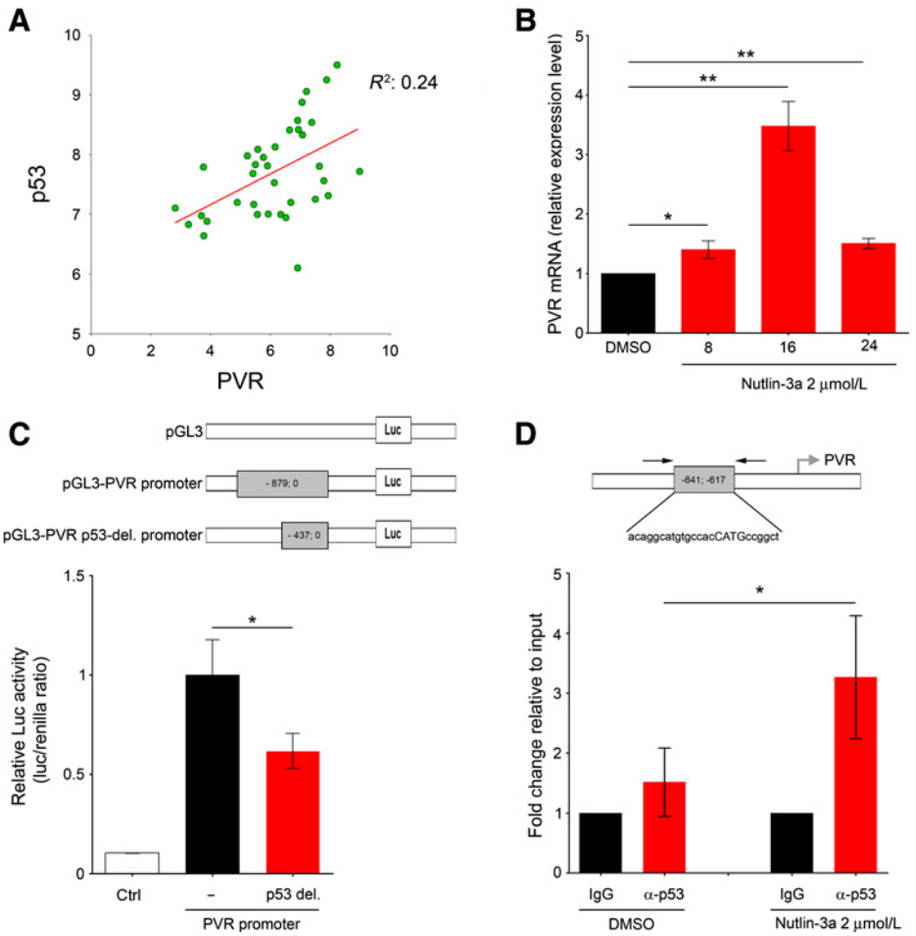

Figure 2.

p53 acts as a direct transcription factor on *PVR* promoter. **A,** Correlation between p53 and PVR expression from NanoString analysis performed in 36 neuroblastoma patients from our institute. R^2 is shown. **B,** LA-N-5 cells were treated with 2 μmol/L of Nutlin-3a for the indicated time points or with DMSO as control. Total mRNA was isolated, and *PVR* mRNA evaluated by qPCR. Summary of four independent experiments is shown as mean ± SD; *, $P < 0.05$; **, $P < 0.01$. **C,** Dual luciferase reporter assay performed with two constructs—one containing a region of the *PVR* promoter spanning from nucleotide −879 to the TSS containing six putative p53-binding sites, and another spanning from nucleotide −437 to the TSS and deleted of the four putative p53-binding sites furthest away from the TSS, as shown in Supplementary Fig. S5C and Supplementary Table S1. The empty vector (pGL3-basic) was used as a negative control. Schematic representation of different constructs used is shown. Summary of four experiments of relative luciferase activity of different promoter fragments shown as mean ± SEM; *, $P < 0.05$. Data were normalized with respect to the renilla activity. *P* value, compared with *PVR* promoter and *PVR* p53-deleted promoter (two-tailed unpaired Student *t* test). **D,** Binding of p53 to p53-binding site in the *PVR* gene promoter in DMSO and Nutlin-3a–treated LAN-5 cells by ChIP assay. The amount of immunoprecipitated chromatin bound by either isotype control (IgG) or p53 (IP) was quantified by real-time PCR with primers amplifying a specific *PVR* gene promoter region. The sequence and the position of this region are reported. Specific signals were set relative to those obtained for the chromatin input. Summary of three ChIP independent experiments is shown as mean ± SD; *, $P < 0.05$. *P* value, compared with DMSO and Nutlin-3a–treated neuroblastoma cell lines (two-tailed unpaired Student *t* test).

3a and NK cells, and had a significantly higher number than that seen in NK cell–treated mice (**Fig. 4E** and **F**; Supplementary Fig. S9). This finding indicated that the immunomodulatory effect of Nutlin-3a on neuroblastoma cells promoted a higher infiltration and retention of NK cells in the tumor masses. These data were consistent with the evidence that the combined treatment of Nutlin-3a and adoptive transfer of NK cells may efficiently control the tumor growth in neuroblastoma-bearing NSG mice (**Fig. 4A–D**).

Nutlin-3a enhances the susceptibility of primary neuroblastoma spheroids to NK cell–mediated killing

Finally, to investigate the immunomodulatory effect of Nutlin-3a on human primary neuroblastoma cells, tumor cells were isolated from BM aspirates of 26 neuroblastoma patients (**Table 1**). Both the number of tumor cells and the ability to grow in culture were found to directly correlate with a poor prognosis, as evaluated by the stage, subtype, *MYCN* or *ALK* status, and patient follow-up (**Table 1**). From 18 of the 26 patient BM samples, we obtained a number of tumor cells greater than 1×10^6/mL. Tumor cells of 8 patients grew in monolayer adherence similarly to neuroblastoma cell lines, and neuroblastoma tumor cells obtained from patient 1 (p1, with metastatic disease and *MYCN* and *ALK* amplification; **Fig. 5** and **Table 1**) formed spheroids. Nutlin-3a significantly enhanced the expression of ligands for both NKG2D and DNAM-1 receptors in primary neuroblastoma cells compared with DMSO-treated control cells (**Fig. 5A**; Supplementary Fig. S10). NK-cell functional

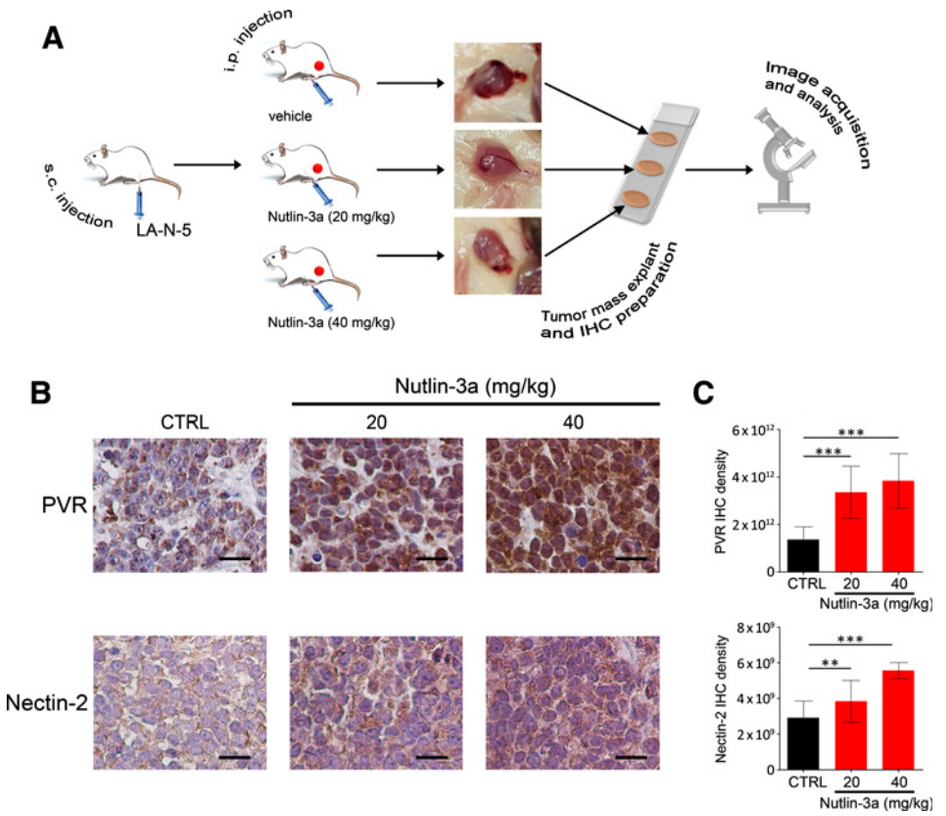

Figure 3.

Nutlin-3a induces the expression of PVR and Nectin-2 in neuroblastoma xenografts. **A,** LA-N-5–bearing NSG mice were treated i.p. with vehicle (CTRL) or Nutlin-3a at 20 mg/kg (drug dose/mouse body weight) or 40 mg/kg doses every 2 days for 2 weeks. Groups of five NSG mice for each condition were assessed. Mice were sacrificed at the end of the treatment, and tumor masses were formaldehyde fixed and paraffin embedded. Blocks were cut into 3-μm sections. Tissue slides from vehicle and Nutlin-3a at 20 mg/kg and at 40 mg/kg masses were mounted on the same slide and stained for antibodies tested in control tissues (Supplementary Fig S6A). Images were acquired by optical microscope, and density measured by ImageJ software. **B,** Representative PVR and Nectin-2 staining in LA-N-5 tissues from NSG mice. Nuclei are counterstained with hematoxylin (blue). Original magnification, ×20. Scale bars, 30 mm. **C,** IHC density was measured in 10 independent areas on four independent slides for each condition, and the mean ± SD of integrated density are reported in the histogram. *P* value, compared with vehicle and Nutlin-3a–treated neuroblastoma cell lines (two-tailed unpaired Student *t* test); **, $P < 0.01$; ***, $P < 0.001$.

assays with spheroids obtained from p1 showed that, after 16 hours of coculture with NK cells, the Nutlin-3a–pretreated neuroblastoma spheroids were significantly more disaggregated than the DMSO-pretreated spheroids, as evaluated by optical microscopic analysis (**Fig. 5B** and **C**). In Nutlin-3a–pretreated spheroids cocultured with NK cells, tumor cells showed significantly enhanced apoptosis compared with DMSO-pretreated spheroids cocultured with NK cells (**Fig. 5D**). Altogether, these data indicated that Nutlin-3a significantly upregulated ligands recognized by NK-ARs in primary neuroblastoma tumor cells, thus boosting the NK cell–mediated killing of tumor spheroids obtained by a particularly aggressive form of neuroblastoma.

Discussion

NK cells play a crucial role in neuroblastoma immunotherapy, as evaluated in both preclinical and clinical studies (44, 45). However, neuroblastoma adopts several immune-evasion strategies, such as the downregulation of both MHC class I and ligands for NK-ARs, thus rendering neuroblastoma cells resistant to both T and NK cells, respectively (3, 5, 6, 44). The identification of anticancer drugs having additional advantages of immunomodulatory effects, such as the induction of ligands for NK-ARs, remains challenging (46). We previously showed that the expression of the activating ligands for NKG2D and DNAM-1 is inversely correlated with that of MYCN in high-risk neuroblastoma patients (3). We also found that JQ1 treatment, although able to efficiently downregulate the expression of MYCN, fails to upregulate activating ligands, thus making neuroblastoma cell lines refractory to NK cell–mediated recognition (13). Of note, none of the chemotherapeutic drugs tested, commonly used in the clinical treatment of neuroblastoma, showed such effects on different neuroblastoma cell lines (47). Therefore, in the search of more efficient and less toxic therapeutic approaches (48, 49), new strategies are needed to support and enhance the NK cell–based immunotherapy of neuroblastoma.

Herein, we provided evidence of the immunomodulatory effects of Nutlin-3a, which lead to significantly increased NK cell–mediated killing and shrinkage of p53-wild-type neuroblastoma cells, evaluated *in vitro* and *in vivo* in a murine model. Mechanistically, this effect occurred through the Nutlin-3a–mediated rescue of p53 function, resulting in a significant induction of NKG2D receptor ligands ULBP1, ULBP2/5/6, and ULBP3 and DNAM-1 receptor ligands PVR and Nectin-2 on neuroblastoma cells. We also demonstrated that p53 was a direct transcription factor for PVR ligand.

Several Nutlin-3a analogues are currently under clinical investigation in various types of tumors (clinicaltrial.gov). Nutlin-3a is nontoxic for normal cells (50, 51), thus appearing as a suitable tool for tumor therapy. Interestingly, pediatric tumors are very often p53-wild-type at diagnosis (52), and therefore are potential therapeutic targets for Nutlin-3a–based treatment (20). Although Nutlin-3a has been reported to induce both proapoptotic effects and cell-growth arrest in tumor cells (16–18, 20, 23), including neuroblastoma (21, 23–27), its immunomodulatory activity at low doses, as revealed in this study, had never been reported.

We found a significant correlation between p53 and PVR expression at the transcriptional level in neuroblastoma patients, whereas no correlation was detected with the other ligands, except a trend for ULBP3. By using two different approaches, namely, luciferase

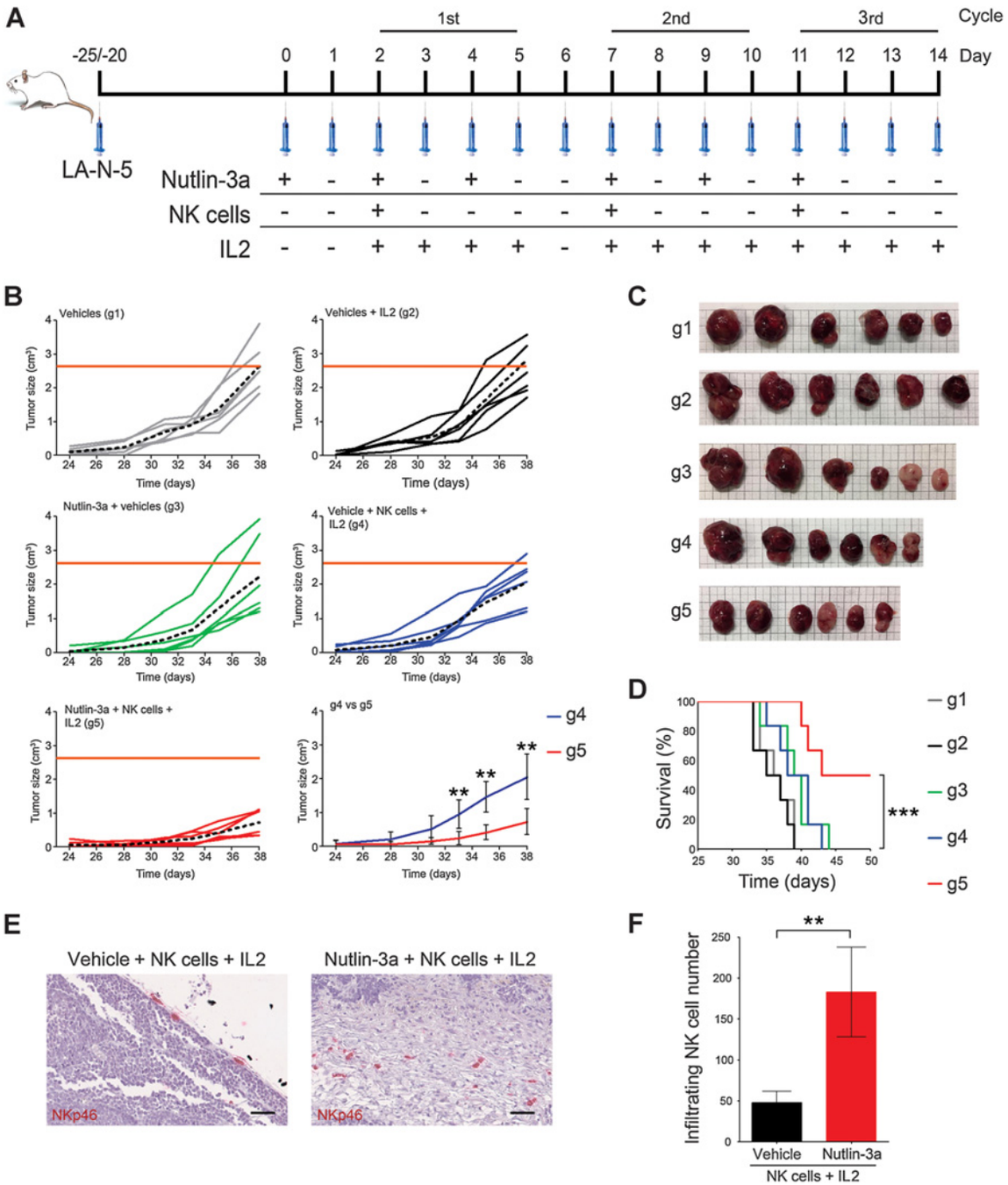

Figure 4.

Nutlin-3a boosts NK cells against neuroblastoma cell lines *in vivo*, thus controlling tumor growth and improving mouse survival. NSG mice were injected subcutaneously into the right flank with LA-N-5 cell line (six mice per group) and treated with vehicles (g1); vehicles plus IL2 (g2); Nutlin-3a and vehicles (g3); vehicles and peritumoral NK cells plus i.p. IL2 (g4); and Nutlin-3a combined with NK cells plus IL2 (g5). **A,** Treatment scheme. **B,** Tumor size was monitored by caliper, and the tumor growth curve generated for each mouse. Mean tumor growth for each group is indicated by black dashed lines. The orange bar indicates the threshold relative to tumor size mean of the vehicle group. Mean tumor size of Nutlin-3a combined with NK cells plus IL2 (g5) compared with that of the NK cells plus IL2 group (g4) is shown as mean ± SD; **, $P < 0.01$, in the last graph. A representative of three independent experiments is reported. **C,** Tumor masses explanted at day 35 of treatment for g1–g5. Images of one representative experiment of three are reported. **D,** Overall survival of mice treated as in **A**. Mice were sacrificed when tumor masses reached almost 2 cm^3. A representative of three independent experiments is reported. Mean ± SD; ***, $P < 0.001$. **E,** Representative examples of NKp46 staining in LA-N-5 tumors treated as indicated. Red, NKp46-expressing cells. Nuclei were counterstained with hematoxylin (blue). Original magnifications, ×20. Scale bars, 30 μm. Details of representative slides are reported (whole representative slides in Supplementary Fig. S8). **F,** Summary of tumor-infiltrating NK cells quantified by ImageJ on five slides of three independent masses is reported as mean ± SD; **, $P < 0.01$. *P* value (two-tailed unpaired Student *t* test).

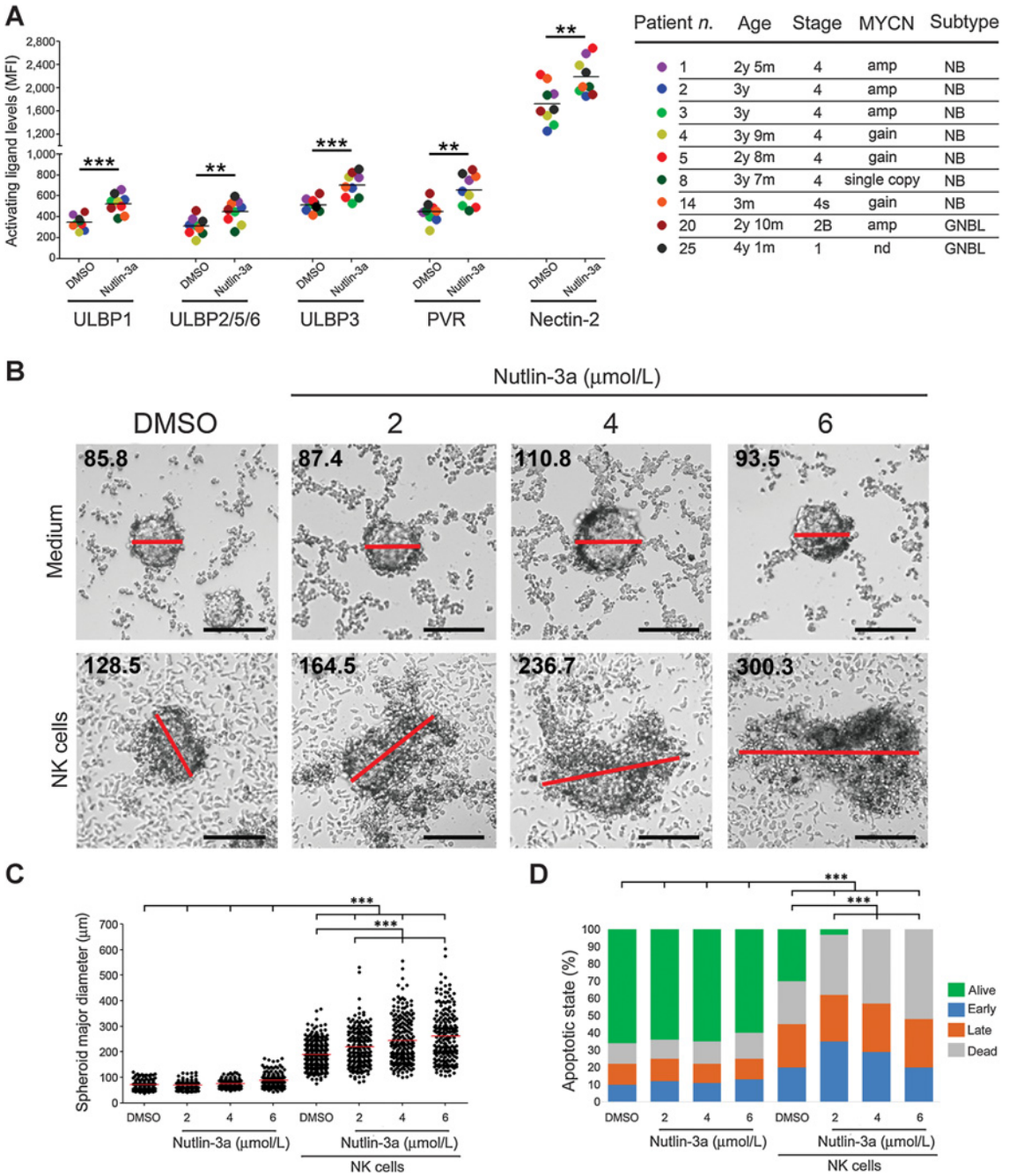

Figure 5.

Nutlin-3a induces the expression of ligands for NK-ARs in primary neuroblastoma cells, thus rendering spheroids more susceptible to NK cell–mediated lysis. **A,** Primary neuroblastoma cells obtained from BM aspirates of nine neuroblastoma patients were treated with 2 μmol/L of Nutlin-3a, or DMSO as control, for 48 hours, and the surface expression of ligands for NK-ARs was analyzed by flow cytometry. Each dot represents the mean of three independent staining for each independent primary neuroblastoma cells; horizontal bars, mean; **, $P < 0.01$; ***, $P < 0.001$. Some peculiar diagnostic characteristic of these neuroblastoma patients are reported in the associated table. amp, amplified; GNBL, ganglioneuroblastoma; MFI, mean fluorescence intensity; NB, neuroblastoma; nd, not determined. **B,** Primary neuroblastoma cells obtained from patient 1 (p1) were grown in culture as spheroids and were treated with three different doses of Nutlin-3a (2, 4, and 6 μmol/L), or DMSO as control, for 48 hours and evaluated by optical microscopy. After Nutlin-3a treatment, 200×10^3 NK cells/well were added, and after 16 hours, the spheroids were reanalyzed by optical microscopy. The spheroid diameter was analyzed by ImageJ. Representative images of spheroids treated with Nutlin-3a or DMSO before and after the addition of NK cells are presented. The major diameter of spheroids is indicated by red bars, and the values (μm) are reported in each panel. Original magnifications, ×20. Scale bars, 100 μm. **C,** Summary of spheroid major diameters evaluated in 230 spheroids; horizontal bars, mean; *** $P < 0.001$. **D,** Spheroids were harvested and stained for Annexin V and PI to evaluate the apoptotic state before and after NK-cell addition by flow cytometry. The mean percentage of cells in the early phase of apoptosis (Annexin V^+PI^-, blue column), of cells in the late phase (Annexin V^+PI^+, orange column), of dead cells (Annexin V^-PI^+, gray column), and of alive cells (Annexin V^-PI^-, green column) for each condition analyzed in four independent wells is reported in the stacked histogram; ***, $P < 0.001$. P value (two-tailed unpaired Student t test).

reporter assays and ChIP assays, we demonstrated that p53 was a direct transcription factor for the *PVR* ligand, by specifically binding the related gene promoter. Whereas p53 is already known to act as a transcription factor for *ULBP1* and *ULBP2* ligands by binding p53-responsive elements to related gene introns (8), no information is known about the regulatory mechanism of p53 on *Nectin2*. However, given the lack of correlation with p53 at the transcriptional level, as well as the absence of p53 binding sites on the ligand promoter according to bioinformatic prediction, it is conceivable that the induced expression of the other ligands, other than PVR, was independent of the direct p53 binding to the related promoters and that p53 may act indirectly through other target genes. In this context, Nutlin-3a is known not only to induce cell-cycle arrest and apoptosis in p53-wild-type neuroblastoma cells, but also to trigger premature cellular senescence and neuronal differentiation (23), conditions that may contribute to induced expression of ligands for NK-ARs (53). Of note, cell-cycle arrest and senescence are known to be triggered by the expression of *p21*, a p53 target gene (54). Consistently, we found that the functional rescue of p53 at preapoptotic doses of Nutlin-3a resulted in a significant accumulation of p21 in neuroblastoma cell lines. Therefore, we can hypothesize that Nutlin-3a–induced p21 expression may trigger an early phase of cell-growth arrest, thus contributing to enhance the expression of activating ligands.

In the clinical setting, the concentration of Nutlin-3a or its analogues can vary according to the drug pharmacokinetic distribution and clearance, mechanisms that occur in specific tissues following drug administration (55–57). Therefore, in addition to inducing cell-cycle arrest and apoptosis at cytotoxic concentrations, Nutlin-3a can have an immunomodulatory effect at preapoptotic concentrations, depending on the drug distribution, thus strengthening its clinical use, and that of its analogues, for the treatment of cancer. In conclusion, our work indicated that Nutlin-3a treatment with the adoptive transfer of NK cells might constitute an effective combinatorial strategy for NK cell–based immunotherapy to treat p53-wild-type tumors, such as neuroblastoma.

Authors' Disclosures

L. Cifaldi reports grants and personal fees from Italian Ministry of Health during the conduct of the study. No disclosures were reported by the other authors.

Authors' Contributions

I. Veneziani: Conceptualization, data curation, software, formal analysis, investigation, and methodology. **P. Infante:** Data curation, formal analysis, investigation, and methodology. **E. Ferretti:** Resources, formal analysis, investigation, methodology, and project administration. **O. Melaiu:** Software, formal analysis, investigation, methodology, writing–review and editing. **C. Battistelli:** Software, formal analysis, investigation, and methodology. **V. Lucarini:** Investigation and methodology. **M. Compagnone:** Investigation and methodology. **C. Nicoletti:** Methodology. **A. Castellano:** Resources, data curation, and validation. **S. Petrini:** Software, formal analysis, investigation, and methodology. **M. Ognibene:** Software, investigation, and methodology. **A. Pezzolo:** Resources, software, investigation, and methodology. **L. Di Marcotullio:** Resources, formal analysis, and methodology. **R. Bei:** Formal analysis, writing–review and editing. **L. Moretta:** Supervision, validation, writing–original draft, writing–review and editing. **V. Pistoia:** Conceptualization, supervision, and validation. **D. Fruci:** Resources, data curation, formal analysis, validation, investigation, methodology, writing–original draft, writing–review and editing. **V. Barnaba:** Resources, formal analysis, writing–original draft, writing–review and editing. **F. Locatelli:** Resources, supervision, validation, writing–original draft, writing–review and editing. **L. Cifaldi:** Conceptualization, resources, data curation, software, formal analysis, supervision, funding acquisition, validation, investigation, visualization, methodology, writing–original draft, project administration, writing–review and editing.

Acknowledgments

This work was supported by the Italian Ministry of Health (Rome, Italy) Grant GR-2011-02352151 to L. Cifaldi and Associazione Italiana per la Ricerca sul Cancro (AIRC, Milan, Italy) "Investigator Grant" #18495 to D. Fruci, both #15199 and #19939 to V. Barnaba, and #20801 to L. Di Marcotullio. This research was also supported by fellowships from the Fondazione Veronesi (to O. Melaiu and V. Lucarini).

The costs of publication of this article were defrayed in part by the payment of page charges. This article must therefore be hereby marked *advertisement* in accordance with 18 U.S.C. Section 1734 solely to indicate this fact.

Received April 20, 2020; revised September 17, 2020; accepted December 4, 2020; published first December 10, 2020.

References

1. Maris JM. Recent advances in neuroblastoma. N Engl J Med 2010;362:2202–11.
2. Raffaghello L, Prigione I, Airoldi I, Camoriano M, Morandi F, Bocca P, et al. Mechanisms of immune evasion of human neuroblastoma. Cancer Lett 2005;228:155–61.
3. Brandetti E, Veneziani I, Melaiu O, Pezzolo A, Castellano A, Boldrini R, et al. MYCN is an immunosuppressive oncogene dampening the expression of ligands for NK-cell-activating receptors in human high-risk neuroblastoma. Oncoimmunology 2017;6:e1316439.
4. Vanichapol T, Chutipongtanate S, Anurathapan U, Hongeng S. Immune escape mechanisms and future prospects for immunotherapy in neuroblastoma. Biomed Res Int 2018;2018:1812535.
5. Marcus A, Gowen BG, Thompson TW, Iannello A, Ardolino M, Deng W, et al. Recognition of tumors by the innate immune system and natural killer cells. Adv Immunol 2014;122:91–128.
6. Raffaghello L, Prigione I, Airoldi I, Camoriano M, Levreri I, Gambini C, et al. Downregulation and/or release of NKG2D ligands as immune evasion strategy of human neuroblastoma. Neoplasia 2004;6:558–68.
7. Nanbakhsh A, Pochon C, Mallavialle A, Amsellem S, Bourhis JH, Chouaib S. c-Myc regulates expression of NKG2D ligands ULBP1/2/3 in AML and modulates their susceptibility to NK-mediated lysis. Blood 2014;123:3585–95.
8. Textor S, Fiegler N, Arnold A, Porgador A, Hofmann TG, Cerwenka A. Human NK cells are alerted to induction of p53 in cancer cells by upregulation of the NKG2D ligands ULBP1 and ULBP2. Cancer Res 2011;71:5998–6009.
9. Carr-Wilkinson J, O'Toole K, Wood KM, Challen CC, Baker AG, Board JR, et al. High frequency of p53/MDM2/p14ARF pathway abnormalities in relapsed neuroblastoma. Clin Cancer Res 2010;16:1108–18.
10. Agarwal S, Milazzo G, Rajapakshe K, Bernardi R, Chen Z, Barbieri E, et al. MYCN acts as a direct co-regulator of p53 in MYCN amplified neuroblastoma. Oncotarget 2018;9:20323–38.
11. Slack A, Chen Z, Tonelli R, Pule M, Hunt L, Pession A, et al. The p53 regulatory gene MDM2 is a direct transcriptional target of MYCN in neuroblastoma. Proc Natl Acad Sci U S A 2005;102:731–6.
12. Carr J, Bell E, Pearson AD, Kees UR, Beris H, Lunec J, et al. Increased frequency of aberrations in the p53/MDM2/p14(ARF) pathway in neuroblastoma cell lines established at relapse. Cancer Res 2006;66:2138–45.
13. Veneziani I, Fruci D, Compagnone M, Pistoia V, Rossi P, Cifaldi L. The BET-bromodomain inhibitor JQ1 renders neuroblastoma cells more resistant to NK cell-mediated recognition and killing by downregulating ligands for NKG2D and DNAM-1 receptors. Oncotarget 2019;10:2151–60.
14. Vassilev LT, Vu BT, Graves B, Carvajal D, Podlaski F, Filipovic Z, et al. In vivo activation of the p53 pathway by small-molecule antagonists of MDM2. Science 2004;303:844–8.
15. Tovar C, Rosinski J, Filipovic Z, Higgins B, Kolinsky K, Hilton H, et al. Small-molecule MDM2 antagonists reveal aberrant p53 signaling in cancer: implications for therapy. Proc Natl Acad Sci U S A 2006;103:1888–93.

16. Kojima K, Konopleva M, Samudio IJ, Shikami M, Cabreira-Hansen M, McQueen T, et al. MDM2 antagonists induce p53-dependent apoptosis in AML: implications for leukemia therapy. Blood 2005;106:3150–9.
17. Secchiero P, Barbarotto E, Tiribelli M, Zerbinati C, di Iasio MG, Gonelli A, et al. Functional integrity of the p53-mediated apoptotic pathway induced by the nongenotoxic agent nutlin-3 in B-cell chronic lymphocytic leukemia (B-CLL). Blood 2006;107:4122–9.
18. Stuhmer T, Chatterjee M, Hildebrandt M, Herrmann P, Gollasch H, Gerecke C, et al. Nongenotoxic activation of the p53 pathway as a therapeutic strategy for multiple myeloma. Blood 2005;106:3609–17.
19. Coll-Mulet L, Iglesias-Serret D, Santidrian AF, Cosialls AM, de Frias M, Castano E, et al. MDM2 antagonists activate p53 and synergize with genotoxic drugs in B-cell chronic lymphocytic leukemia cells. Blood 2006; 107:4109–14.
20. Miyachi M, Kakazu N, Yagyu S, Katsumi Y, Tsubai-Shimizu S, Kikuchi K, et al. Restoration of p53 pathway by nutlin-3 induces cell cycle arrest and apoptosis in human rhabdomyosarcoma cells. Clin Cancer Res 2009;15:4077–84.
21. Gamble LD, Kees UR, Tweddle DA, Lunec J. MYCN sensitizes neuroblastoma to the MDM2-p53 antagonists Nutlin-3 and MI-63. Oncogene 2012;31:752–63.
22. Hasegawa H, Yamada Y, Iha H, Tsukasaki K, Nagai K, Atogami S, et al. Activation of p53 by Nutlin-3a, an antagonist of MDM2, induces apoptosis and cellular senescence in adult T-cell leukemia cells. Leukemia 2009;23:2090–101.
23. Van Maerken T, Speleman F, Vermeulen J, Lambertz I, De Clercq S, De Smet E, et al. Small-molecule MDM2 antagonists as a new therapy concept for neuroblastoma. Cancer Res 2006;66:9646–55.
24. Van Maerken T, Ferdinande L, Taildeman J, Lambertz I, Yigit N, Vercruysse L, et al. Antitumor activity of the selective MDM2 antagonist nutlin-3 against chemoresistant neuroblastoma with wild-type p53. J Natl Cancer Inst 2009;101: 1562–74.
25. Van Maerken T, Vandesompele J, Rihani A, De Paepe A, Speleman F. Escape from p53-mediated tumor surveillance in neuroblastoma: switching off the p14 (ARF)-MDM2-p53 axis. Cell Death Differ 2009;16:1563–72.
26. Peirce SK, Findley HW. The MDM2 antagonist nutlin-3 sensitizes p53-null neuroblastoma cells to doxorubicin via E2F1 and TAp73. Int J Oncol 2009;34: 1395–402.
27. Barbieri E, Mehta P, Chen Z, Zhang L, Slack A, Berg S, et al. MDM2 inhibition sensitizes neuroblastoma to chemotherapy-induced apoptotic cell death. Mol Cancer Ther 2006;5:2358–65.
28. Brodeur GM, Pritchard J, Berthold F, Carlsen NL, Castel V, Castelberry RP, et al. Revisions of the international criteria for neuroblastoma diagnosis, staging, and response to treatment. J Clin Oncol 1993;11:1466–77.
29. Shimada H, Ambros IM, Dehner LP, Hata J, Joshi VV, Roald B, et al. The international neuroblastoma pathology classification (the Shimada system). Cancer 1999;86:364–72.
30. Mathew P, Valentine MB, Bowman LC, Rowe ST, Nash MB, Valentine VA, et al. Detection of MYCN gene amplification in neuroblastoma by fluorescence in situ hybridization: a Pediatric Oncology Group study. Neoplasia 2001;3:105–9.
31. Cifaldi L, Romania P, Falco M, Lorenzi S, Meazza R, Petrini S, et al. ERAP1 regulates natural killer cell function by controlling the engagement of inhibitory receptors. Cancer Res 2015;75:824–34.
32. Pende D, Marcenaro S, Falco M, Martini S, Bernardo ME, Montagna D, et al. Anti-leukemia activity of alloreactive NK cells in KIR ligand-mismatched haploidentical HSCT for pediatric patients: evaluation of the functional role of activating KIR and redefinition of inhibitory KIR specificity. Blood 2009;113: 3119–29.
33. Fontana L, Fiori ME, Albini S, Cifaldi L, Giovinazzi S, Forloni M, et al. Antagomir-17–5p abolishes the growth of therapy-resistant neuroblastoma through p21 and BIM. PLoS One 2008;3:e2236.
34. Romania P, Cifaldi L, Pignoloni B, Starc N, D'Alicandro V, Melaiu O, et al. Identification of a genetic variation in ERAP1 aminopeptidase that prevents human cytomegalovirus miR-UL112–5p-mediated immunoevasion. Cell Rep 2017;20:846–53.
35. Martens UM, Zijlmans JM, Poon SS, Dragowska W, Yui J, Chavez EA, et al. Short telomeres on human chromosome 17p. Nat Genet 1998;18:76–80.
36. Ferlicot S, Youssef N, Feneux D, Delhommeau F, Paradis V, Bedossa P. Measurement of telomere length on tissue sections using quantitative fluorescence in situ hybridization (Q-FISH). J Pathol 2003;200:661–6.
37. Canela A, Vera E, Klatt P, Blasco MA. High-throughput telomere length quantification by FISH and its application to human population studies. Proc Natl Acad Sci U S A 2007;104:5300–5.
38. Waggott D, Chu K, Yin S, Wouters BG, Liu FF, Boutros PC. NanoStringNorm: an extensible R package for the pre-processing of NanoString mRNA and miRNA data. Bioinformatics 2012;28:1546–8.
39. Stricker TP, Morales La Madrid A, Chlenski A, Guerrero L, Salwen HR, Gosiengfiao Y, et al. Validation of a prognostic multi-gene signature in high-risk neuroblastoma using the high throughput digital NanoString nCounter system. Mol Oncol 2014;8:669–78.
40. Melaiu O, Chierici M, Lucarini V, Jurman G, Conti L, De Vito R, et al. Cellular and gene signatures of tumor-infiltrating dendritic cells and natural-killer cells predict prognosis of neuroblastoma. Nature Commun 2020;11:5992.
41. Elmore S. Apoptosis: a review of programmed cell death. Toxicol Pathol 2007;35: 495–516.
42. Cifaldi L, Doria M, Cotugno N, Zicari S, Cancrini C, Palma P, et al. DNAM-1 activating receptor and its ligands: how do viruses affect the NK cell-mediated immune surveillance during the various phases of infection? Int J Mol Sci 2019; 20:3715.
43. Chang YH, Connolly J, Shimasaki N, Mimura K, Kono K, Campana D. A chimeric receptor with NKG2D specificity enhances natural killer cell activation and killing of tumor cells. Cancer Res 2013;73:1777–86.
44. Melaiu O, Lucarini V, Cifaldi L, Fruci D. Influence of the tumor microenvironment on NK cell function in solid tumors. Front Immunol 2019;10:3038.
45. McNerney KO, Karageorgos SA, Hogarty MD, Bassiri H. Enhancing neuroblastoma immunotherapies by engaging iNKT and NK cells. Front Immunol 2020;11:873.
46. Cifaldi L, Locatelli F, Marasco E, Moretta L, Pistoia V. Boosting natural killer cell-based immunotherapy with anticancer drugs: a perspective. Trends Mol Med 2017;23:1156–75.
47. Veneziani I, Brandetti E, Ognibene M, Pezzolo A, Pistoia V, Cifaldi L. Neuroblastoma cell lines are refractory to genotoxic drug-mediated induction of ligands for NK cell-activating receptors. J Immunol Res 2018;2018:4972410.
48. Ladenstein R, Weixler S, Baykan B, Bleeke M, Kunert R, Katinger D, et al. Ch14.18 antibody produced in CHO cells in relapsed or refractory Stage 4 neuroblastoma patients: a SIOPEN phase 1 study. mAbs 2013;5:801–9.
49. Richman SA, Milone MC. Neurotoxicity associated with a high-affinity GD2 CAR-response. Cancer Immunol Res 2018;6:496–7.
50. Carvajal D, Tovar C, Yang H, Vu BT, Heimbrook DC, Vassilev LT. Activation of p53 by MDM2 antagonists can protect proliferating cells from mitotic inhibitors. Cancer Res 2005;65:1918–24.
51. Shangary S, Qin D, McEachern D, Liu M, Miller RS, Qiu S, et al. Temporal activation of p53 by a specific MDM2 inhibitor is selectively toxic to tumors and leads to complete tumor growth inhibition. PNAS 2008;105:3933–8.
52. Pinto EM, Ribeiro RC, Figueiredo BC, Zambetti GP. TP53-associated pediatric malignancies. Genes Cancer 2011;2:485–90.
53. Soriani A, Zingoni A, Cerboni C, Iannitto ML, Ricciardi MR, Di Gialleonardo V, et al. ATM-ATR-dependent up-regulation of DNAM-1 and NKG2D ligands on multiple myeloma cells by therapeutic agents results in enhanced NK-cell susceptibility and is associated with a senescent phenotype. Blood 2009;113: 3503–11.
54. Georgakilas AG, Martin OA, Bonner WM. p21: a two-faced genome guardian. Trends Mol Med 2017;23:310–9.
55. Zhang F, Tagen M, Throm S, Mallari J, Miller L, Guy RK, et al. Whole-body physiologically based pharmacokinetic model for nutlin-3a in mice after intravenous and oral administration. Drug Metab Dispos 2011;39:15–21.
56. Zhao YS, Li C. Mass spectrometry imaging: applications in drug distribution studies. Curr Drug Metab 2015;16:807–15.
57. Puszynski K, Gandolfi A, d'Onofrio A. The pharmacodynamics of the p53-Mdm2 targeting drug Nutlin: the role of gene-switching noise. PLoS Comput Biol 2014;10:e1003991.